NASA/TM—2013-216612

# Application of Advanced Nondestructive Evaluation Techniques for Cylindrical Composite Test Samples

*Richard E. Martin*
*Cleveland State University, Cleveland, Ohio*

*Donald J. Roth and Jonathan A. Salem*
*Glenn Research Center, Cleveland, Ohio*

December 2013

# NASA STI Program . . . in Profile

Since its founding, NASA has been dedicated to the advancement of aeronautics and space science. The NASA Scientific and Technical Information (STI) program plays a key part in helping NASA maintain this important role.

The NASA STI Program operates under the auspices of the Agency Chief Information Officer. It collects, organizes, provides for archiving, and disseminates NASA's STI. The NASA STI program provides access to the NASA Aeronautics and Space Database and its public interface, the NASA Technical Reports Server, thus providing one of the largest collections of aeronautical and space science STI in the world. Results are published in both non-NASA channels and by NASA in the NASA STI Report Series, which includes the following report types:

- TECHNICAL PUBLICATION. Reports of completed research or a major significant phase of research that present the results of NASA programs and include extensive data or theoretical analysis. Includes compilations of significant scientific and technical data and information deemed to be of continuing reference value. NASA counterpart of peer-reviewed formal professional papers but has less stringent limitations on manuscript length and extent of graphic presentations.

- TECHNICAL MEMORANDUM. Scientific and technical findings that are preliminary or of specialized interest, e.g., quick release reports, working papers, and bibliographies that contain minimal annotation. Does not contain extensive analysis.

- CONTRACTOR REPORT. Scientific and technical findings by NASA-sponsored contractors and grantees.

- CONFERENCE PUBLICATION. Collected papers from scientific and technical conferences, symposia, seminars, or other meetings sponsored or cosponsored by NASA.

- SPECIAL PUBLICATION. Scientific, technical, or historical information from NASA programs, projects, and missions, often concerned with subjects having substantial public interest.

- TECHNICAL TRANSLATION. English-language translations of foreign scientific and technical material pertinent to NASA's mission.

Specialized services also include creating custom thesauri, building customized databases, organizing and publishing research results.

For more information about the NASA STI program, see the following:

- Access the NASA STI program home page at *http://www.sti.nasa.gov*

- E-mail your question to *help@sti.nasa.gov*

- Fax your question to the NASA STI Information Desk at 443–757–5803

- Phone the NASA STI Information Desk at 443–757–5802

- Write to:
  STI Information Desk
  NASA Center for AeroSpace Information
  7115 Standard Drive
  Hanover, MD 21076–1320

NASA/TM—2013-216612

# Application of Advanced Nondestructive Evaluation Techniques for Cylindrical Composite Test Samples

*Richard E. Martin*
*Cleveland State University, Cleveland, Ohio*

*Donald J. Roth and Jonathan A. Salem*
*Glenn Research Center, Cleveland, Ohio*

National Aeronautics and
Space Administration

Glenn Research Center
Cleveland, Ohio 44135

December 2013

This work was sponsored by the Fundamental Aeronautics Program at the NASA Glenn Research Center.

*Level of Review*: This material has been technically reviewed by technical management.

Available from

NASA Center for Aerospace Information
7115 Standard Drive
Hanover, MD 21076–1320

National Technical Information Service
5301 Shawnee Road
Alexandria, VA 22312

Available electronically at http://www.sti.nasa.gov

# Application of Advanced Nondestructive Evaluation Techniques for Cylindrical Composite Test Samples

Richard E. Martin
Cleveland State University
Cleveland, Ohio 44115

Donald J. Roth and Jonathan A. Salem
National Aeronautics and Space Administration
Glenn Research Center
Cleveland, Ohio 44135

## Abstract

Two nondestructive methods were applied to composite cylinder samples pressurized to failure in order to determine manufacturing quality and monitor damage progression under load. A unique computed tomography (CT) image processing methodology developed at NASA Glenn Research Center was used to assess the condition of the as-received samples while acoustic emission (AE) monitoring was used to identify both the extent and location of damage within the samples up to failure. Results show the effectiveness of both of these methods in identifying potentially critical fabrication issues and their resulting impact on performance.

## Introduction

Composite materials are widely used in many high-performance structures. The successful replacement of traditional materials with composites is due to their high specific strength and stiffness coupled with cost effectiveness. Although these materials are attractive because of the properties mentioned, there is still a need to better understand potential issues regarding manufacturing-related defects and their effects on mechanical properties (Refs. 1 and 2). In particular, improper fiber alignment, porosity and delaminations may impact response to design loads and should be identified prior to placing a component in service. To address these issues, a number of nondestructive evaluation tools have been applied to composites to identify performance and life limiting defects with varying degrees of success (Ref. 3). Inspection of composites is more difficult than examination of traditional metallic components because of the non-uniform material architecture. Inspection is even more challenging when complex shapes must be examined. This study seeks to identify and apply advanced NDE techniques that can be used as tools for material development and eventually applied to component testing. In particular two NDE methods, advanced computed tomography (CT) and acoustic emission (AE), were applied to cylindrical composite samples to identify manufacturing-related defects and track both damage progression and location as the samples were loaded to failure. This coupled approach is used to help determine if material defects found prior to testing have a significant impact on the response of the material under load. The following sections describe the samples used, the methods employed, and the experimental findings.

# Experimental Setup

## Test Samples

Three 6 in. (152.4 mm) long carbon-epoxy composite tube samples were used in this experiment. A representative sample is shown in Figure 1. Samples were fabricated using a preform of overbraided layers of triaxial braid carbon fiber with the axial tows of the braid running in the axial direction of the tube. The finished composite was formed by resin transfer molding using a 3502 epoxy resin. Final dimensions were an inner diameter of 4 in. (102 mm) and a wall thickness of 0.140 in. (3.6 mm). Visual examination of the samples indicated discontinuities on the outer surface of the cylinder at the locations where the outer mold sections joined together as well as some visible fiber misalignment on the sample exterior surfaces.

## Mechanical Testing

Tube samples were loaded to failure using a pressurized tube test method, shown schematically in Figure 2, which produces a good approximation of pure transverse tension in the central region where failure initiates. This method yields strength values comparable to axial strength values, which is what would be expected because of the balance fiber architecture. Loading of the pressurized plug in the tube was accomplished by using a servo-hydraulic load frame in stroke control to provide the necessary compressive load. Along with load information, strain data was collected using a digital image correlation (DIC) system with a surface speckle pattern that is given 3D coordinates which are tracked from one image to another. From the calculated 3D deformations, a wide array of deformation based measurements can be calculated. The speckle pattern consists of random high contrast black and white speckles applied with aerosol paint.


Figure 1.—Representative cylindrical composite test sample.

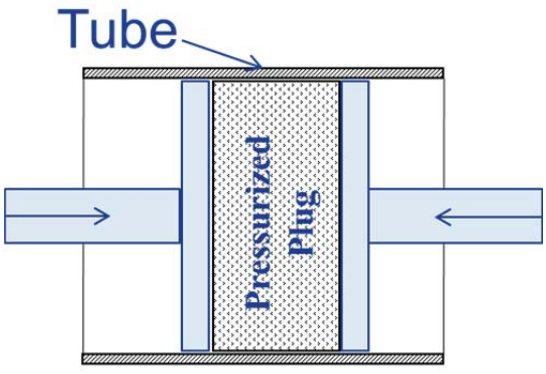


Figure 2.—Schematic of mechanical test setup.

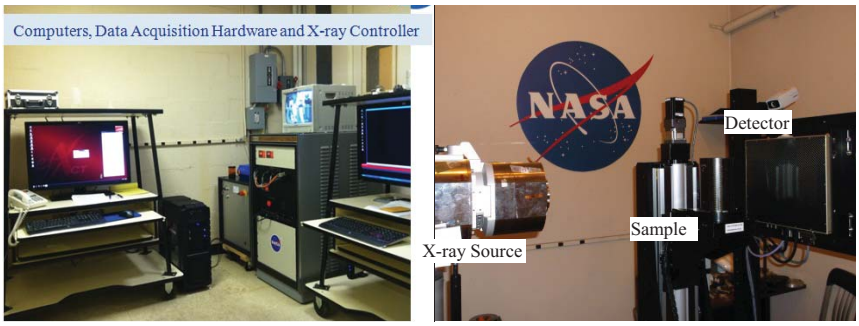


Figure 3.—Microfocus X-ray CT system.

## Computed Tomography (CT)

### Acquisition

Prior to mechanical testing, the samples were examined using the commercially available Microfocus X-ray Computed Tomography (μCT) system shown in Figure 3. The system uses a microfocus x-ray cone beam source and a fine pitch flat panel digital detector to capture multiple full-field projections at discrete rotational increments. Following acquisition, the projection data was software reconstructed using the Feldkamp filtered backprojection technique (Ref. 4) to provide a series of cross-sectional slices that can be rendered as a volume. Specifically, the system employed for this testing utilized an X-ray WorX XWT-225-THE microfocus X-ray 225 kV source coupled with a Dexela 2923 Detector (0.0748 mm pitch, 29×23 cm area, and 3888×3072 pixel elements). Data acquisition, motion control and reconstruction were accomplished using software from NSI, Inc.

### Data Analysis

Traditionally, 3-D CT data visualization is performed by examining orthogonal slices from volumetric data. Depending on the geometry of the part, these views can be limiting in terms of providing useful information regarding flaws. In the case of the composite tubes used in this study, cross-sections tend to only provide thin strips of data corresponding to the thickness of the sample and offer little information regarding fiber orientation, ply layup or flaw morphology (Fig. 4). In many instances large flaws can be completely overlooked due to their relatively small size against the background in the cross-sectional view. Also, due to the high pixel resolution of the detector used, resulting CT reconstructions tend to be very large. In the case of this study, data sets with over 2700 cross-sectional images and a total size of nearly 14 Gb were generated. Paging through such a large number of high resolution images tends to be impractical for an inspector. As an alternative, volume renderings of the data can offer some insight regarding the condition of the part (Fig. 5), but results tend to be sensitive to the settings used to generate the volume rendering (i.e., contrast, transparency) and can also lead to missed flaws.

In the case of cylindrical samples, is has been shown to be beneficial to examine the volumetric CT data as a series of circumferential slices rather than traditional orthogonal projections (Ref. 5). Using this technique, 2-D “sheets” of data can be visualized from interior to exterior rather than simply looking at thin cross-sections. As an added benefit, for relatively thin cylindrical samples, the resulting number of images is significantly reduced when compared to the original data set. In order to accomplish this unique visualization approach, NASA GRC has developed a dedicated cylindrical CT data unwrapper/reslicer software program (CT-CURS) (Ref. 5). The program automatically performs all of the necessary pre-processing functions such as histogram matching and slice alignment necessary to accurately reconstruct the resliced data. Using the known voxel resolution of the acquired data set, the software enables the user to accurately measure features of interest in either the resliced view or traditional cross-sectional view. Additional features are also available to perform advanced image processing and feature identification on the data sets. CT-CURS is available for download by U.S. citizens at https://sr.grc.nasa.gov/public/project/86/.

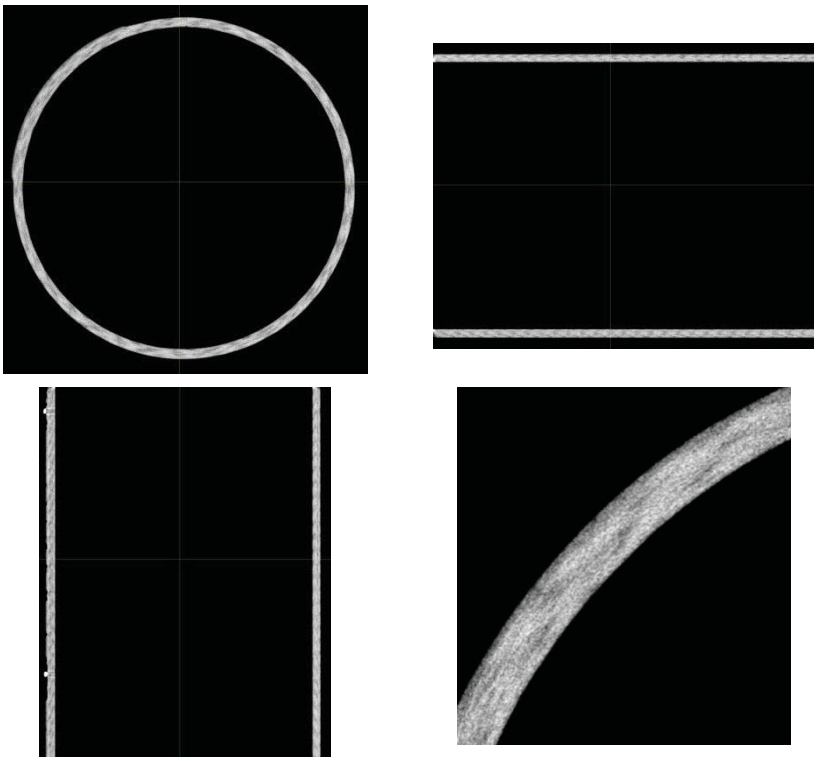

Figure 4.—Typical orthogonal projection results for composite tube sample. Enlarged view of horizontal cross-section shown in bottom right.

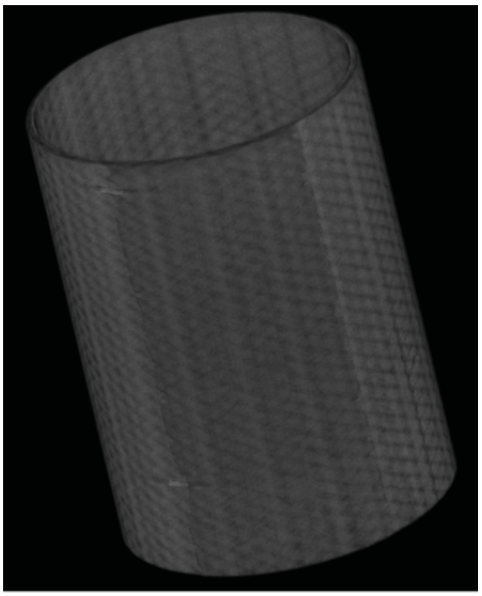

Figure 5.—Typical volume rendering result for composite tube sample.

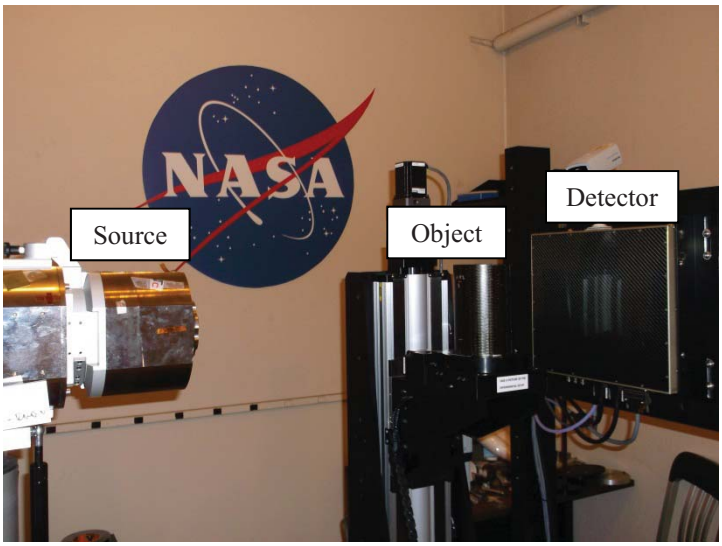


Figure 6.—CT experimental setup.

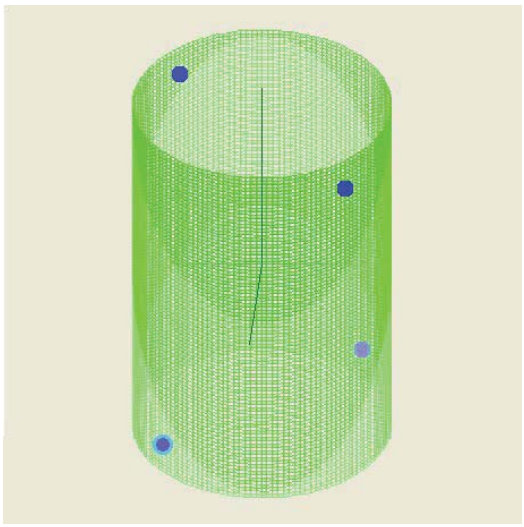

Figure 7.—Acoustic emission sensor placement.

### CT Test Setup

Composite tube samples were placed between the x-ray source and detector in a position to provide maximum magnification while keeping the gage section of the sample within the detector field of view (Fig. 6). A source-to-object distance of 540 mm and a source to detector distance of 800 mm resulted in a magnification factor of approximately 1.5. X-ray source power used was 15 W (75 kV, 200 μA) with a 0.254 mm copper filter in front of the source. Projection images were captured every 0.2° (1800 views) with a 4 frame average at each position. The voxel size of the reconstructed data sets was approximately 50 μm. Thin clay markers were placed on the surface of the sample to locate both the zero position of the part and the mark the gage length of the burst test area.

## Acoustic Emissions

### Acquisition

Acoustic emission data was collected during the test using a commercially available four channel acoustic emission system from Digital Wave Corporation. Four broadband (100 kHz-3 MHz) sensors were coupled to the sample using vacuum grease at 90° increments and alternating from top to bottom as shown in Figure 7 in order to cover the entire sample area. Waveform data for each AE event was collected at 5 MHz and stored for later processing. Events detected by a single sensor during loading triggers data acquisition on all sensor channels simultaneously, enabling location calculations to be performed based on AE arrival times. Load data from the test rig was collected along with the AE event data for later correlation. Prior to testing, a series of lead break tests were performed to determine wave speeds used for location calculations.

### Data Processing

Acquired signals were post-processed using the AE system software. Processing steps included automated and manual filtering of the data to eliminate low energy noise events and events occurring after sample failure. Cylindrical location of the AE events based on arrival times and experimentally determined wave speeds was then performed and saved along with load data. For better visualization of the results, spreadsheet macros were written to post-process the AE and load data, and to present the results in a more useable format for analysis.

# Results

## Mechanical Testing Results

Mechanical response for the three composite tube samples is shown in Figure 8 with a photo of a failed sample shown in Figure 9. Strain response data in the transverse direction indicates a nearly linear response to failure with failure strains in the range of 1.7 to 1.9 percent based on DIC data. One of the samples, 1038B, did show a stiffer response and a higher failure load than the other samples. Full field DIC results near failure show non-uniformity in the strain field. An example of this behavior is shown in Figure 10.

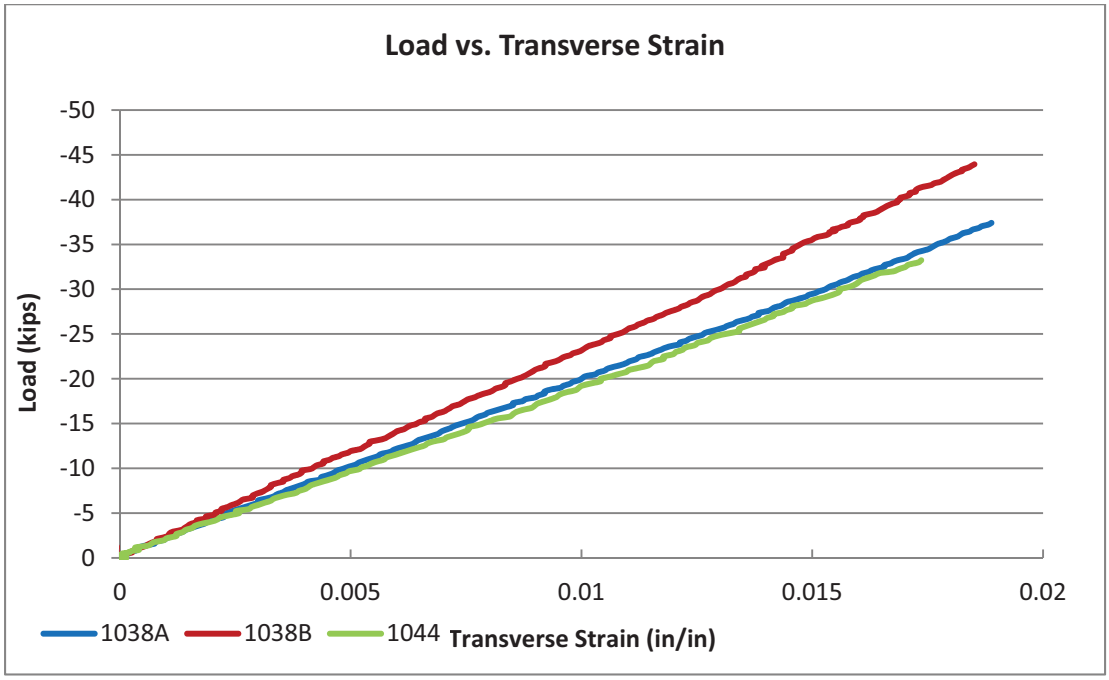


Figure 8.—Load-strain response for samples tested to failure.

Figure 9.—Photograph of failed sample 1038A.

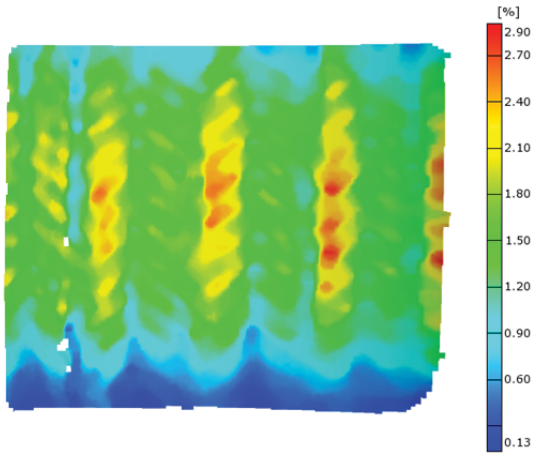


Figure 10.—Full field transverse strain response for sample 1038A near failure.

## AE Results

A summary of the cumulative acoustic emission response for the three samples is shown in Figure 11. All three of the samples exhibited a similar response with an initiation of AE activity around 4,000 lb followed by a nearly linear increase of activity starting at 10,000 lb and continuing until failure much like the load-strain response shown previously. As expected, the sample with the higher failure load, 1038B, resulted in a higher amount of total AE activity.

Results from post-processing of the AE data in terms of location are shown in Figures 12 to 14. Location of the individual events in both the axial and circumferential directions over the load history were calculated and plotted. All of the samples appear to show the same trends in terms of location. In the axial direction, AE activity initially begins in a narrow region within the gage region of the sample. As the load increases, the distribution of AE activity begins to widen and extend slightly beyond the edges of the gage region where it remains until reaching failure load. All three samples also contained a small amount of activity near the ends of the sample which is most likely due to noise from the load frame and fixturing.

AE event activity in the circumferential direction also displays a noticeable trend. During the loading history of each of the samples, there is a background level of AE activity detected over the entire circumference of the sample starting at the initiation load. Coupled with this background activity, there are one or two locations on each sample where AE events are concentrated. These peaks begin to form at the earliest stages of activity and continue until failure. In all three cases, the location with the highest peaks can be associated with the eventual failure location suggesting that the location of damage leading to failure occurs early in the loading process. Other significant peaks in the data correlate well with the locations of the mold lines of the cylinder.

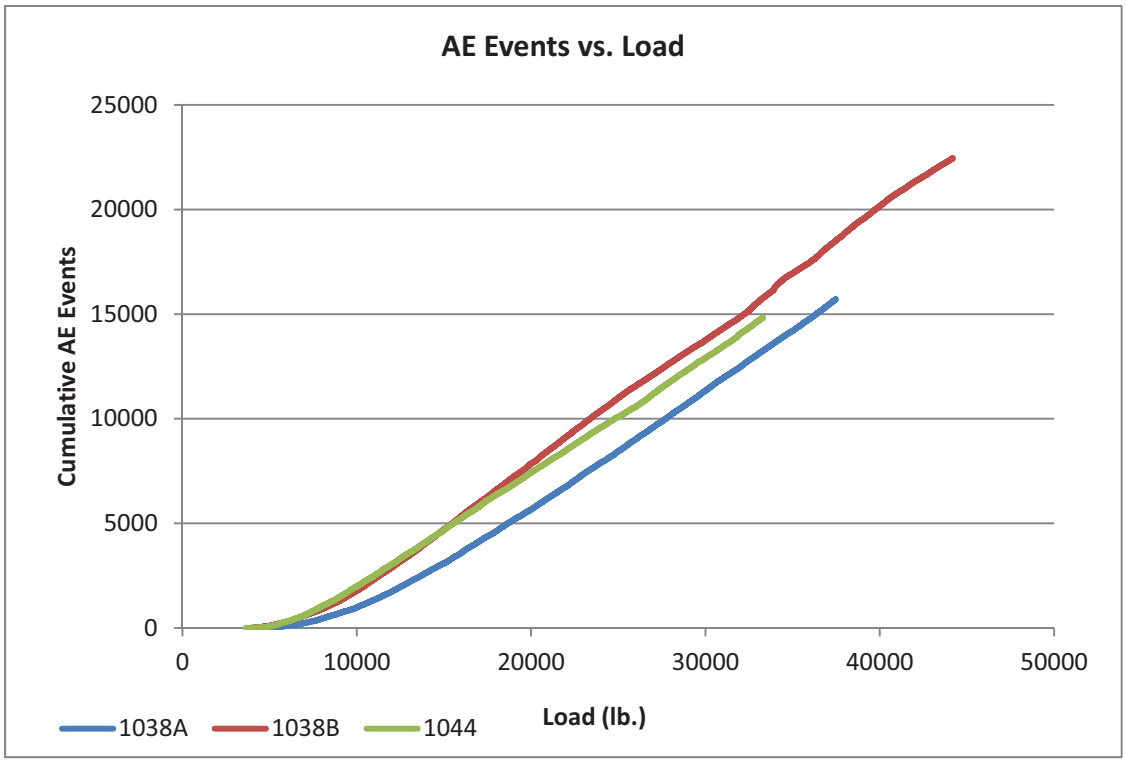


Figure 11.—Cumulative acoustic emission activity as a function of load.

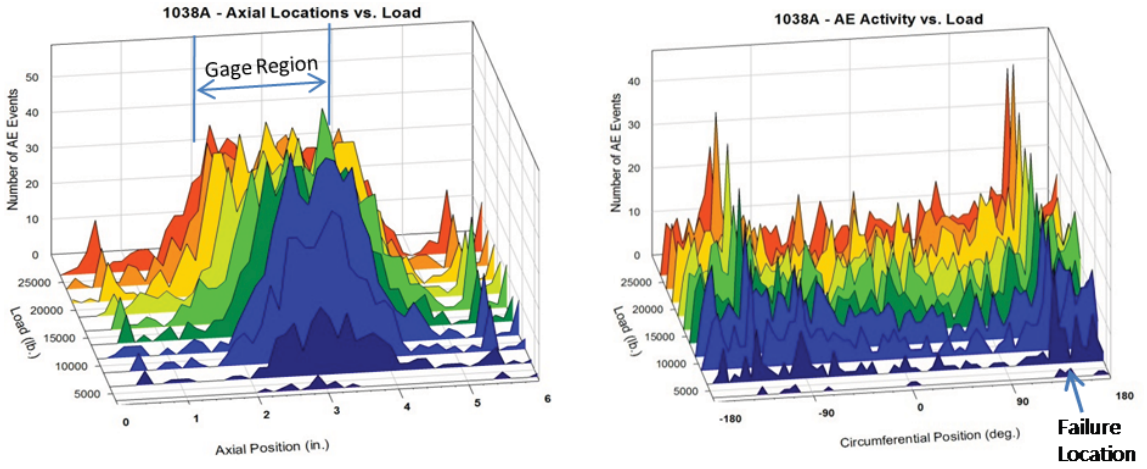


Figure 12.—Axial and circumferential location data for sample 1038A.

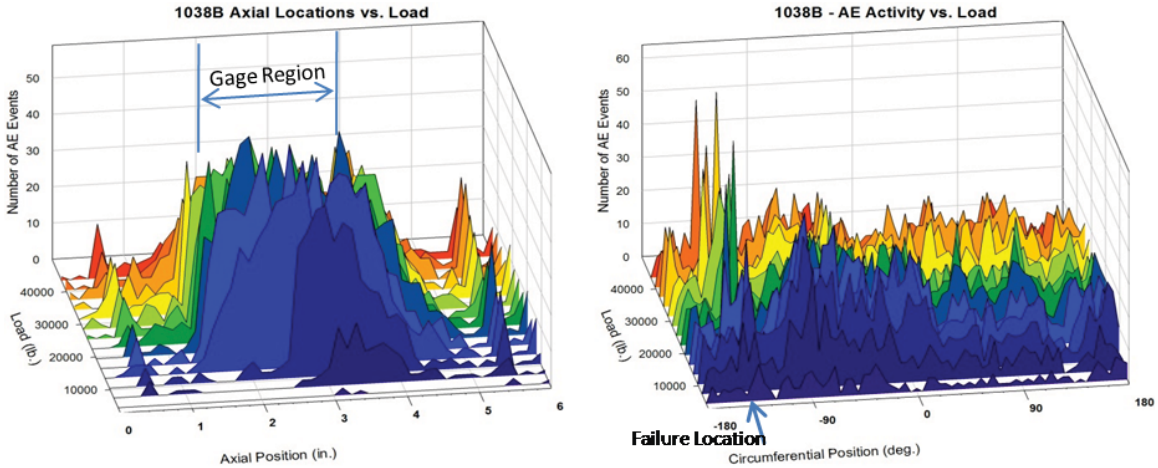


Figure 13.—Axial and circumferential location data for sample 1038B.

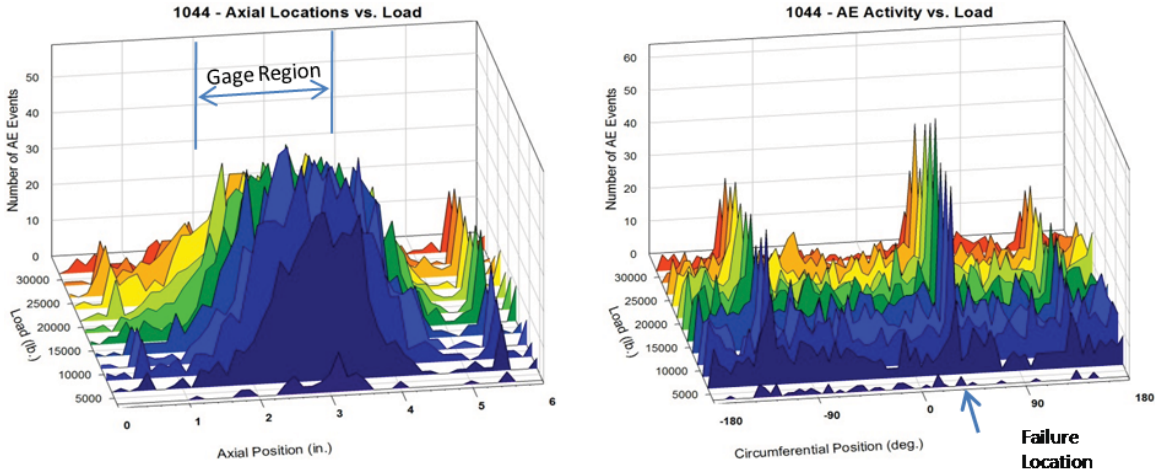


Figure 14.—Axial and circumferential location data for sample 1044.

## CT Results

Figures 15 to 17 show the CT results following the unwrap/reslice procedure. For each of the samples, two circumferential locations are shown. The red circle in the small cross-sectional view indicates the radial depth of the resliced image. A location near the surface is shown to highlight variations at the mold lines due to manufacturing. A second circumferential slice is shown at a location below the surface to demonstrate the ability of the reslice technique to highlight material architecture, locate variations related to manufacturing and identify subsurface defects. Along with each of the images, a marker identifying the failure location is provided.

In the case of the first sample, 1038A, failure occurred near the mold line opposite the zero markers on the sample. Discontinuities on the outer surface are clearly visible in the resliced image near the outer surface and by visually examining the sample. Below the surface the fiber architecture appears to be uniform with no significant indications of manufacturing related flaws such as porosity. In contrast, sample 1038B shows a significant amount of non-uniformity in the fiber layout both at the surface and throughout the thickness of the sample. Issues such as waviness in both the axial and bias tows can be clearly seen distributed around the entire sample circumference and concentrated mainly in the top half of the sample coupled with the mold line discontinuities previously observed. No significant indications of porosity or resin rich regions below the surface were identified in any of the resliced images. Failure of the sample appears to have initiated between two mold lines as identified in Figure 16. CT results did not identify any specific indication at this location that may point to the root cause of failure. It is interesting to note that this specimen had the highest failure load of the tested samples, implying that mold lines are critical to strength. The final sample, 1044, demonstrated a mold line failure similar to 1038A. Examination of the resliced CT results indicates similar discontinuities associated with the mold line but also shows a line of porosity visible at the sample surface as a long dark line in the axial direction. Below the surface, the same area contains more distributed porosity that appears to follow the bias tow direction and is concentrated at the top of the sample and near the failure location.

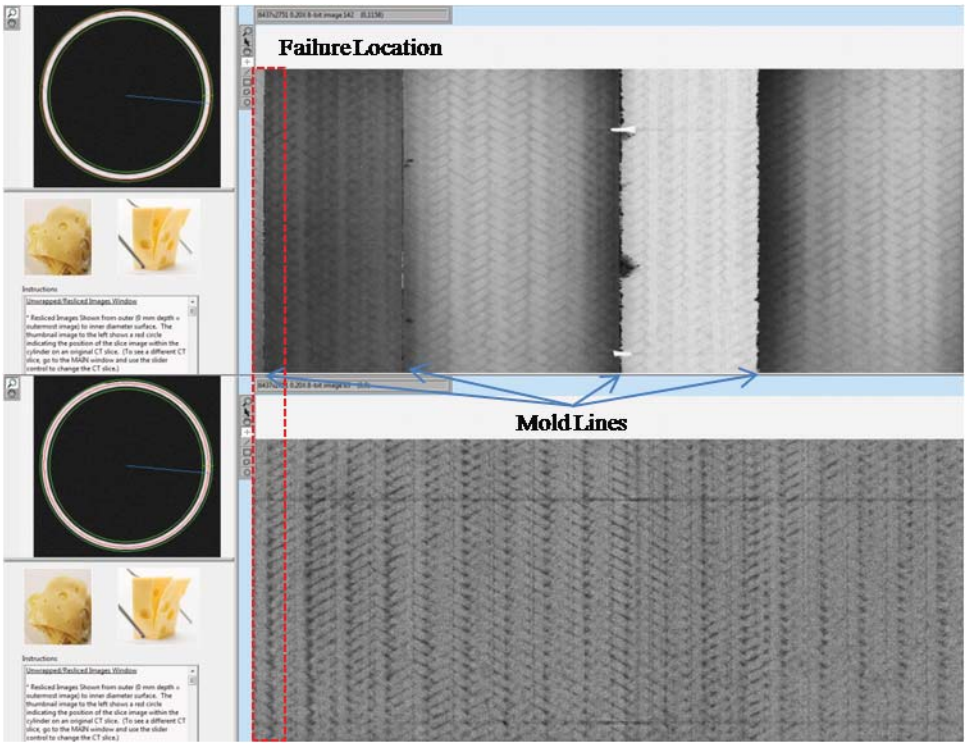


Figure 15.—Sample 1038A CT reslice results.

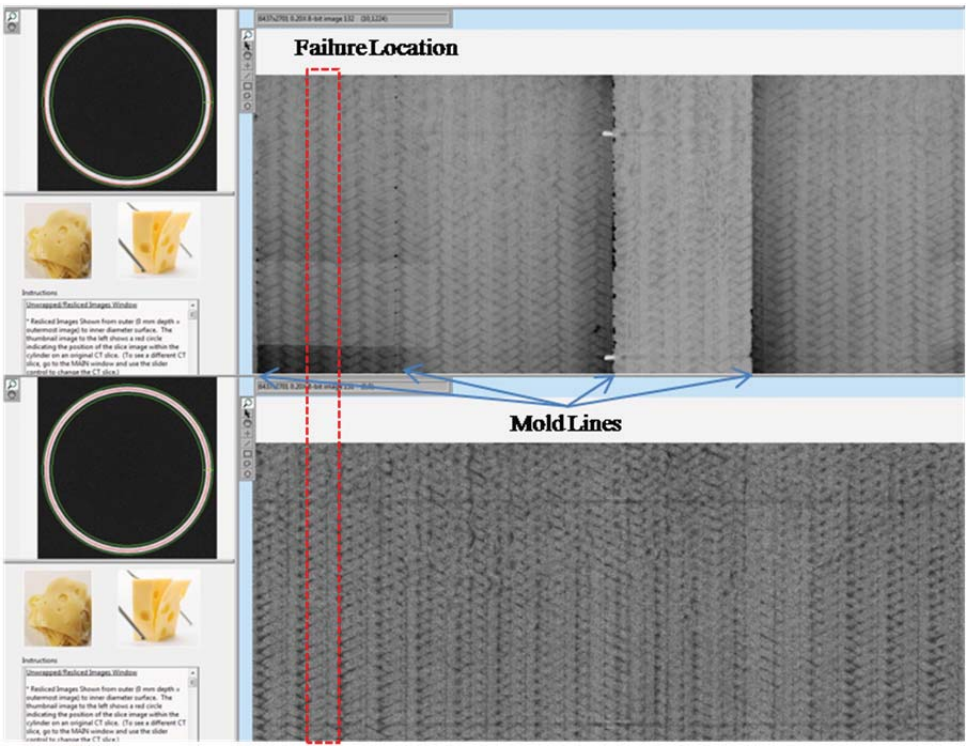


Figure 16.—Sample 1038B CT reslices results. Not nonuniformity at exterior surface and interior positions.

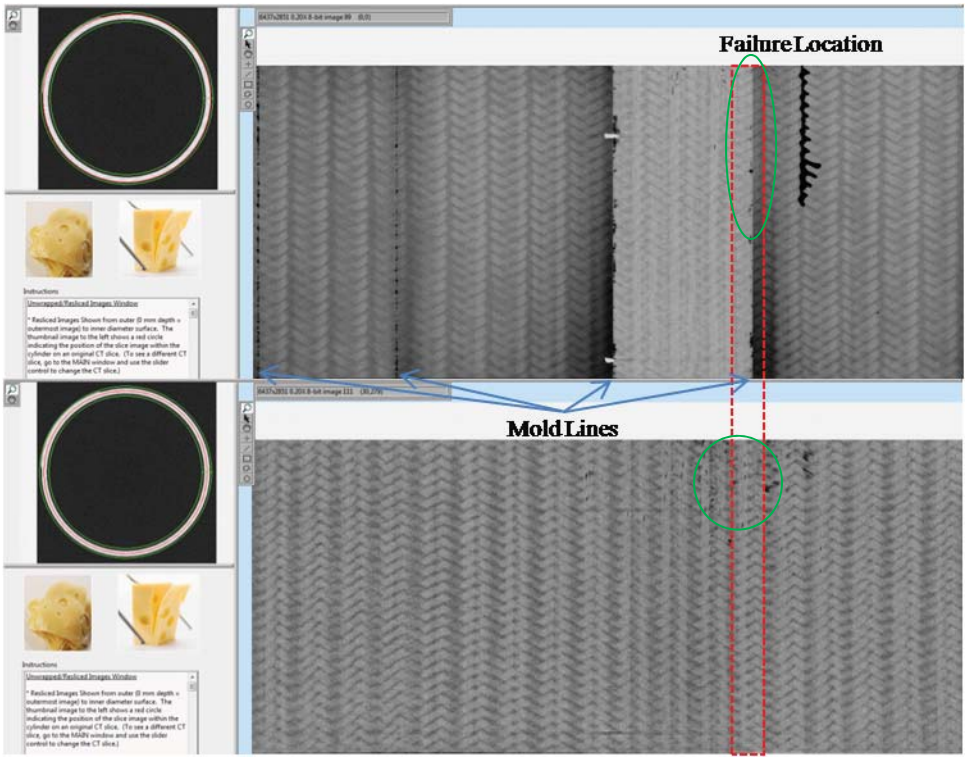


Figure 17.—Sample 1044 CT results. Porosity line shown circled in green.

## Conclusions

Data collected for a series of cylindrical composite tube samples using a high resolution CT system and using advanced image processing tools was analyzed to assess the material in the as received condition and identify potential defects that may affect load capacity. Results of this study demonstrate the ability of the technique to identify manufacturing related issues such as fiber misalignment and subsurface porosity as well as near-surface defects related to the molding process. This type of information can be used to not only improve fabrication methods, but may also identify anomalies that can lead to early failure. In the case of the samples used in this study, mold line discontinuities appear to dominate failure in two out of the three samples with the addition of subsurface porosity as a possible contributor. Issues such as fiber misalignment did not appear to have a significant effect on ultimate strength. In fact, the sample that appeared to have the most non-uniformity in terms of architecture also had the highest failure load.

As a monitoring tool, acoustic emission testing was shown to be an effective way to assess the behavior of the composite samples under load. Information regarding damage initiation loads and damage accumulation rates can be determined from examination of the AE data over the loading history and can be used as a comparison tool in future material development. Processing of the AE data to isolate event locations offers a more detailed picture of damage progression within the material. Coupled with the information gathered by other nondestructive methods such as CT and visual examination, specific issues leading to failure can be identified and used to suggest areas for improvement in both material and component development.

## References


1. Bhat, M.R. and Binoy, M.P. and Surya, N.M. and Murthy, C.R.L. and Engelbart, R.W., "Non-destructive evaluation of porosity and its effect on mechanical properties of carbon fiber reinforced polymer composite materials," Review of Progress in Quantitative Nondestructive Evaluation. Volume 31, 17–22 July 2011, Burlington, VT, pp. 1080–1087.
2. Hsiao H.M., Daniel I.M., "Elastic properties of composites with fiber waviness," Composites Part A: Applied Science and Manufacturing, Volume 27, Issue 10, 1996, Pages 931–941.
3. Vaara, Pauli, and Jukka Leinonen. "Technology Survey on NDT of Carbon-fiber Composites," (2012).
4. Feldkamp, L.A., Davis, L.C., and Kress, J.W., "Practical cone-beam algorithm," J. Opt. Soc. Amer. A6 (1984), 612–619.
5. Roth, D.J., Burke, E.R., Rauser, R.W., and Martin, R.E., "A Novel Automated Method for Analyzing Cylindrical Computed Tomography Data," Extended Abstract Paper Proceedings at Fall 2011 ASNT conference. Palm Springs Convention Center, Palm Springs, California. October 24–28. pp. 139–145.